ELSEVIER

Tectonophysics 274 (1997) 41–59

TECTONOPHYSICS

Velocity field of GPS stations in the Taiwan area

Shui-Beih Yu *, Horng-Yue Chen, Long-Chen Kuo

Institute of Earth Sciences, Academia Sinica, P.O. Box 1-55, Nankang, Taipei, Taiwan

Received 14 February 1996; accepted 20 June 1996

Abstract

The 131 stations of the 'Taiwan GPS Network' were surveyed 4–6 times from 1990 to 1995 with dual-frequency geodetic receivers. The standard deviation of an observed baseline length with its linear trend removed is in the range of 6–10 mm for a 3–120 km long baseline. The average rates of length change for all baselines of the network and those from nine continuously monitoring permanent stations are used in a least squares adjustment to estimate the velocities of the GPS stations relative to Paisha, Penghu, situated at the Chinese continental margin. To the south of Fengping, in the northern Coastal Range, the velocity vectors of stations in Lanhsu, Lutao, and the Coastal Range trend in the directions of 306°–322° with rates of 56–82 mm/yr. In contrast, there is a dramatic decrease in the rates to the north of Fengping. This may be caused by the motion along the NE–SW-trending thrusts which obliquely cut the northern Coastal Range. A discontinuity of about 30 mm/yr in the rates along with a remarkable change in the directions of station velocity is observed across the Longitudinal Valley, then the moving directions gradually shift to the west for the stations in the Western Foothills. In the Kaohsiung–Pingtung coastal area, the station velocities are even directed toward the southwest. To the north of the Peikang High, the velocity vectors of the stations change direction from the west gradually to the north and finally to the east and southeast. Significant NW–SE extensional deformation is found in the Ilan Plain and northern Taiwan. In general, the pattern of the velocity field for GPS stations in the Taiwan area is quite consistent with the directions of present-day tectonic stress.

Keywords: GPS survey; Velocity field; Crustal deformation; Active fault; Taiwan

1. Introduction

The satellite-based navigation system, the Global Positioning System (GPS), has a constellation of 24 satellites with orbits 20,000 km in altitude and orbital periods of about 12 h. It is operated by the U.S. Department of Defense and was originally designed for mainly military purposes. However, more and more civilian users have been applying this new technique in different fields. With the carrier phase signals from GPS satellites being received at two or more sites simultaneously and processing the observed data afterwards, the 3-dimensional relative positions of these sites can be precisely determined. Furthermore, the GPS survey does not require the line-of-sight intervisibility of geodetic stations. It is also much less affected by rugged topography and bad weather conditions. Thus, the GPS survey technique has become an efficient and powerful tool for studying active tectonics and plate motion (e.g. Dixon, 1991; Hager et al., 1991). Now it is possible

* Corresponding author. Tel: +886 2 7839910/416, Fax: +886 2 7839871.

0040-1951/97/$17.00
PII S0040-1951(96)00297-1

to observe crustal motion in an active tectonic region within a short period of only a few years.

The island of Taiwan is a product of the collision between the Luzon arc and the Chinese continental margin (Fig. 1). At present, the collision process is still very active as revealed by the highly active seismicity and rapid crustal movement in and around the area (e.g., Tsai et al., 1977; Wu, 1978; Tsai, 1986; Yu and Lee, 1986; Yu et al., 1992). Analyzing the repeated trilateration and levelling data in the Longitudinal Valley area, eastern Taiwan from 1983 to 1989, Yu and Liu (1989) found that there was up to 20 mm/yr relative vertical motion on both sides of the central segment of the Longitudinal Valley Fault (LVF), which is generally regarded as the suture zone of the Taiwan collision. Relative horizontal motion of approximately 30 mm/yr was also detected along the whole length of the LVF (Yu et al., 1990; Yu and Yu, 1991).

In view of the benefits of the newly developed high-precision GPS survey technique, the original small-aperture trilateration networks were largely expanded to cover the whole island of Taiwan and several offshore islets in 1989 by the Institute of Earth Sciences (IES), Academia Sinica. This large-scale 'Taiwan GPS Network' is now composed of 131 annually surveyed mobile stations and 9 permanent or semi-permanent continuously monitoring stations (Fig. 2). During the period from March 1990 to November 1995 the mobile stations of the network were surveyed 4–6 times with dual frequency geodetic GPS receivers. In the meantime the earliest established continuous stations have been operated since November 1991. The changes in baseline length derived from these repeated and continuous GPS data are utilized to estimate the relative velocities of GPS stations. The preliminary results of this study were presented at the 1995 ACT meeting in Taipei (Yu et al., 1995) and Yu and Chen (1994) reported on the relative motion of the stations in the southern Taiwan GPS Network using the data observed before 1994. In this article we describe the procedures followed in GPS data acquisition and processing and then assess the precision of the observed baseline lengths. The changes in baseline lengths on several distinct geologic provinces are plotted. Finally, the velocity field for the GPS stations in the entire Taiwan GPS Network is presented by incorporating the most recent available data and its tectonic implications are discussed.

2. Tectonic setting

The island of Taiwan is located at the junction between the southeast-facing Ryukyu arc–trench system and the west-facing Luzon arc–Manila trench system (Fig. 1a). The Philippine Sea plate subducts northward beneath the Eurasian plate at the Ryukyu trench and overrides the crust of the South China Sea at the Manila trench which extends from the Philippines to about 20°N off southwestern Taiwan. Between the two opposite-facing Ryukyu and Luzon arcs, the Longitudinal Valley in eastern Taiwan is considered the suture zone of the active collision between the Luzon arc and the Chinese continental margin (e.g., Biq, 1972; Hsu, 1976; Bowin et al., 1978; Wu, 1978; Barrier and Angelier, 1986; Ho, 1986).

Taiwan is generally divided into several geologic provinces (Ho, 1982, 1986) which trend mainly north-northeast (Fig. 1b). From west to east they are: the Penghu Island Group, the Coastal Plain, the Western Foothills, the Central Range, the Longitudinal Valley, and the Coastal Range. The Penghu Island Group in the Taiwan Strait is covered with Pleistocene flood basalt. The Coastal Plain consists of Quaternary alluvial deposits derived from the Western Foothills and the Central Range. The Western Foothills are composed of a thick sequence of shallow marine to shelf sediments from the Late Oligocene, Miocene, to Early Pleistocene. These sediments are deformed by a combination of folds and thrust faults (Fig. 1c) which trend mainly northeast or north and dip toward the east or southeast

Fig. 1. (a) Geodynamic framework around Taiwan: isobaths in metres, large open arrow showing the present direction of plate motion from Seno (1977), thick lines indicating subduction with triangles on overriding side. (b) The geologic provinces in Taiwan: major thrust faults with triangles on the upthrust side, *CKF* = Chukou Fault, *LVF* = Longitudinal Valley Fault. (c) Schematic cross-section of Taiwan (after Teng, 1990). Location shown in (b).

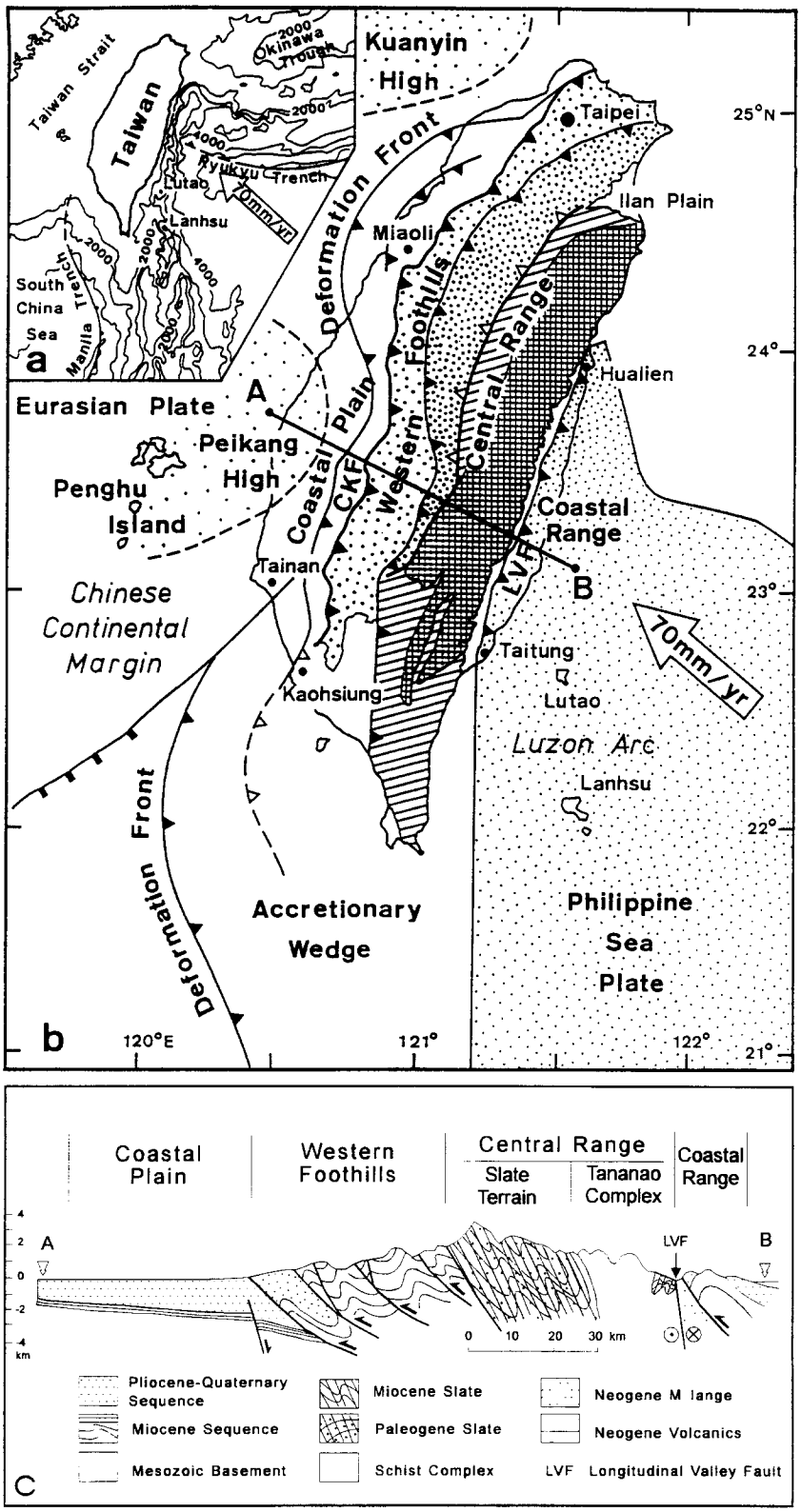
Taiwan Strait
Taiwan
Okinawa Trough
Kuanyin High
Taipei
25°N
Ryukyu Trench
Lutao
10mm/yr
Lanhsu
Ilan Plain
Miaoli
Deformation Front
Foothills
Central Range
South China Sea
Manila Trench
a
24°
Hualien
Eurasian Plate
A
Peikang High
Coastal Plain
CKF
Western
Penghu Island
Coastal Range
Tainan
LVF
B
23°
Chinese Continental Margin
10mm/yr
Taitung
Lutao
Kaohsiung
Luzon Arc
Lanhsu
22°
Deformation Front
Accretionary Wedge
Philippine Sea Plate
b
120°E
121°
122°
21°
Coastal Plain
Western Foothills
Central Range
Slate Terrain
Tananao Complex
Coastal Range
A
LVF
B
0 10 20 30 km
km
Pliocene-Quaternary Sequence
Miocene Sequence
Mesozoic Basement
Miocene Slate
Paleogene Slate
Schist Complex
Neogene M lange
Neogene Volcanics
LVF Longitudinal Valley Fault
C

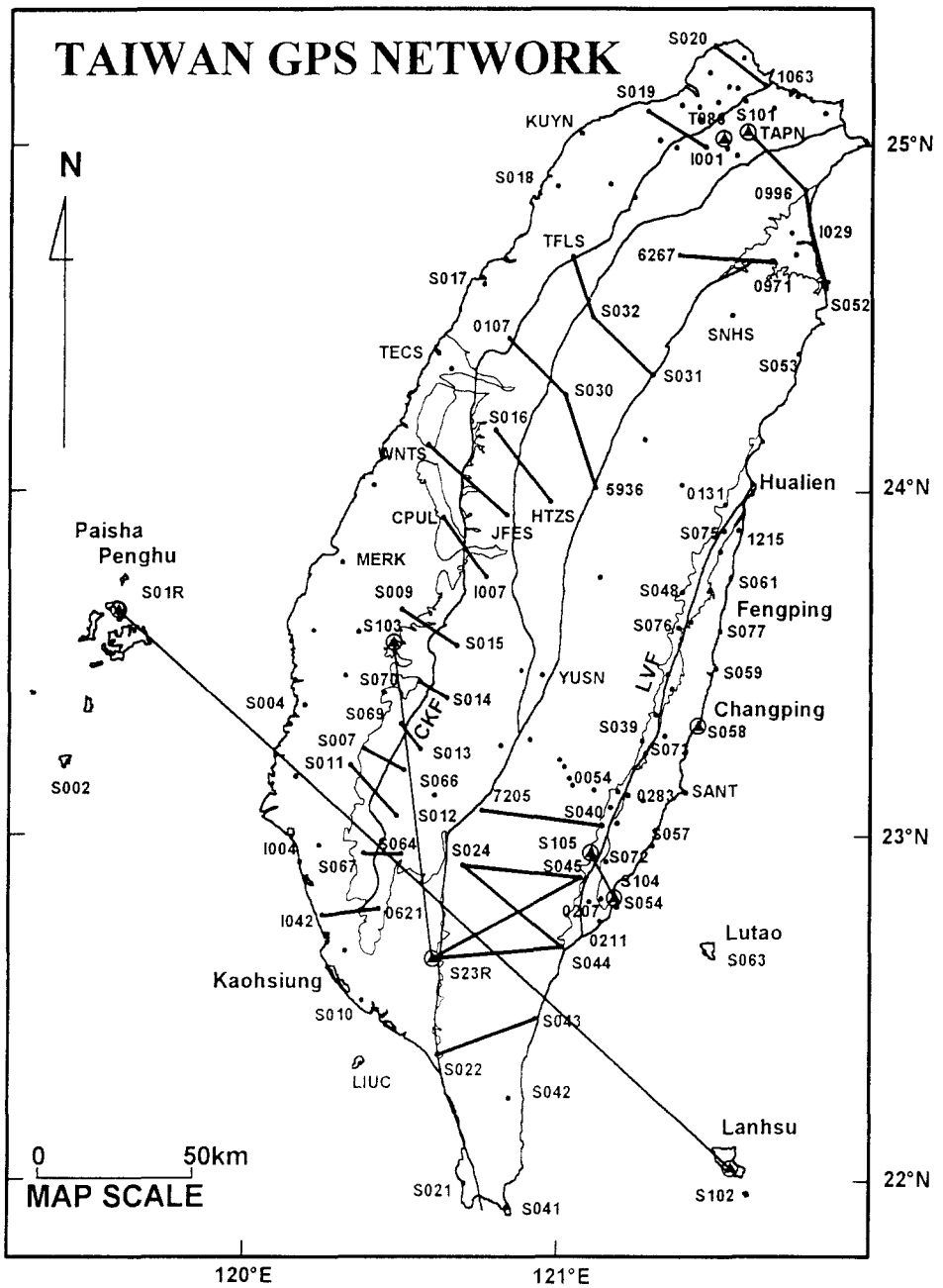

Fig. 2. Taiwan GPS Network. The small dots represent annually surveyed stations, while the solid triangles inside circles denote permanent or semi-permanent stations. The thick lines show major faults, and the straight lines indicate the baselines with their observed lengths plotted.

(Ho, 1976; Suppe, 1980). The Central Range is divided into two parts. The axial ridges and the western flank are underlain by a weakly metamorphosed Cenozoic argillite-slate series, while the eastern flank is composed of the pre-Tertiary basement complex which has been affected by Neogene greenschist facies and higher grades of polyphase Mesozoic–Cenozoic metamorphism.

At the farthest point in the east, the Coastal Range and the two offshore islets, Lutao and Lanhsu, are the northern extension of the Neogene Luzon trough. They are mainly composed of Neogene andesitic volcanic units and associated flyschoid and turbidite sediments. The straight and narrow Longitudinal Valley lies between the Central Range and the Coastal Range and bounded on the east by the well-known Longitudinal Valley Fault (LVF) with the Coastal Range (Fig. 1c). The LVF is a very active high-angle oblique thrust fault with a minor left-lateral strike-slip component (Barrier et al., 1982; Yu and Liu, 1989).

The general structural trends of the Taiwan mountain belt show an elongated S-shape (Fig. 1b). Two major basement highs are recognized: the Kuanyin High to the north and the Peikang High to the south. These basement highs are characterized by tectonic stability, in contrast to the adjacent mobile belt. The Peikang High belongs to the continental lithosphere of Eurasia which underwent normal faulting prior to collision. Geophysical surveys and drilling by the Chinese Petroleum Corporation resulted in the discovery of the Peikang High beneath the Neogene sediments: two wells (PK-2, PK-3) penetrated the basement, with Cretaceous metamorphic rocks, at depths of 1463 m and 1962 m, respectively (Matsumoto, 1965). A well (TL-1) drilled in the Penghu Islands revealed a similar occurrence of mid-Miocene sediments unconformably overlying a Mesozoic basement at a depth of 500 m (Chou, 1969), showing that the main Penghu Islands belong to the offshore extension of the Peikang High. The shape of the basement high, from Peikang to the Penghu Islands, was illustrated by a Bouguer gravity anomaly map (Hsieh and Hu, 1972). The Kuanyin High is located in offshore northwestern Taiwan. This palaeohigh is probably composed of Cretaceous or much older material and is characterized by truncation or no deposition of the Palaeogene and covered with Neogene material (Chen et al., 1994). As in the onshore area, the Kuanyin High is indicated less pronounced than the Peikang High. In the transition zone between the Manila trench and the deformation front of the Taiwan arc–continent collision zone, the frontal portion of the submarine fold and thrust belt is detected along the western flank of the accretionary wedge (Huang et al., 1992; Liu et al., 1993).

3. Data acquisition and processing

Generally, all of the Taiwan GPS Network stations are located at secure sites which exhibit little possibility of local movement and which can be preserved for long periods of up to tens of years. Most of them also have good sky visibility for elevation angles larger than 15°.

Five epoch measurements of the mobile stations for the entire Taiwan GPS Network were conducted during the periods of March to July in 1990, June to November in 1991, May to July in 1993, January to April and November in 1994, as well as March to June and November in 1995. An additional survey was carried out in the densified Taipei GPS Network and the southern Taiwan GPS Network from April to July, 1992. In each survey, four to eight stations were observed simultaneously with dual-frequency geodetic receivers (Trimble 4000 SST Geodetic IIP and 4000 SSE Geodetic Surveyor). A station is usually occupied by more than two sessions, each session being composed of 6–14 h of GPS observations with all available satellites rising higher than a 15° elevation angle being tracked. The sampling interval for data logging is 15 s. The collected data are downloaded from the internal RAM of receivers to a PC hard disk or floppy disks. The raw data of each station are then transferred to the RINEX (Receiver INdependent EXchange) format by a transfer program for use in post-processing.

Four continuously recording permanent GPS stations at Paisha, Penghu (S01R), Taipei (T986 or TAIW), Pingtung (S23R) and Lanhsu (S102) have been operated by the IES, Academia Sinica, since November 1991 (Fig. 2). Another five semi-permanent GPS stations at Changping (S058), Minhsiung (S103), Nankang (S101), Fushan (S104) and Mingyeh (S105), also established by the IES, Academica Sinica, were mostly occupied 7–10 months a year before 1994, a period without field surveys. Since April 1994, however, these five stations have mostly been operated continuously. The station at Taipei, which also serves as one of the IGS (International GPS Service for Geodynamics) global tracking stations, is equipped with a Rogue SNR-800 receiver. The other permanent or semi-permanent stations are equipped with the same models of dual-frequency geodetic receivers as those used in the

epoch field surveys. The sampling interval for data logging is 30 s, and only signals with an elevation angle larger than 15° are recorded. The collected data are downloaded from the internal RAM of receivers by local operators and sent to the IES office in Taipei by Internet daily, or biweekly or monthly by mail.

All available epoch measurements and continuous GPS data are processed with Bernese GPS software v.3.4 which was developed at the Astronomical Institute of the University of Berne, Switzerland (Rothacher et al., 1993). The observed data in each epoch survey are processed session by session to obtain the baseline solutions for all combinations of any two stations in the same session. Since the annual observation period generally spans several months, no attempt is made here to adjust the results from all the sessions of one year to a single solution. For continuous GPS data, daily solutions are computed. The ionosphere-free linear combination of observations at the L1 and L2 frequencies are employed as the basic observable for estimating the station coordinates and baseline solutions. In the 1990 and part of the 1991 surveys, broadcast ephemerides are used in the processing. The precise ephemerides provided by Scripps Institution of Oceanography (SIO) of the University of California, San Diego, U.S.A., are employed in the processing of the 1991–1993 data. Since the beginning of 1994, we have processed the observed data with the official final precise ephemerides distributed by the IGS. Although the baseline solutions estimated from the SIO and IGS ephemerides do not, in fact, reveal any significant differences, in some cases, the solutions using broadcast ephemerides show a larger scattering.

In the data processing, an elevation cutoff angle of 20° is used to reduce any multipath effects and noises. The modified Hopfield (1971) atmospheric zenith delay model with standard atmosphere is utilized to calculate an a-priori model for tropospheric corrections. The standard atmospheric model usually fails to describe the actual meteorological conditions properly at a GPS station during a particular observation session (Brunner and Welsch, 1993). The difference between the actual zenith delay and that calculated from a standard atmospheric model is called the residual zenith delay. We estimate the unknown residual zenith delay once during every 6-h observation session for each station in the least-squares adjustment of the carrier phase observations. The phase ambiguities are firstly estimated as real numbers and then fixed to as many of the closest integers as possible.

The scatter of a series of GPS measurements taken over several years can be employed as an indicator of precision. This long-term repeatability shows the effects of slowly varying systematic errors due to propagation delay, multipath, or fiducial network inconsistencies, and so forth. We assume a steady motion between stations during the five-year period and look at the scatter of data points about a best fit straight line on a plot of the baseline component versus time (Davis et al., 1989). A data point for each baseline is the average of all observations on that baseline within 30 days. Accordingly, the repeatability of a baseline component (east, north, and vertical) or baseline length is the root-mean-square scatter about the linear trend.

The plots of the repeatabilities of length and the north, east and vertical components versus baseline length for all data points obtained from annual surveys are shown in Fig. 3. The baselines range from 3 to 120 km in length, with the majority being less than 50 km. The formalism proposed by Savage and Prescott (1973) is utilized here to describe the precision of the epoch GPS measurements as a function of baseline length:

$$\sigma_L = (a^2 + b^2 \cdot L^2)^{1/2} \tag{1}$$

where σ_L is the standard deviation, L is the baseline length, and a and b are the constant and length-dependent sources of error, respectively. Best fitting curves of Eq. 1 through the repeatability data (shown in Fig. 3) give $a = 5.8 \pm 0.2$ mm, 5.9 ± 0.2 mm, 6.7 ± 0.4 mm, 25.0 ± 1.1 mm, and $b = 0.07 \pm 0.01$ ppm, 0.08 ± 0.01 ppm, 0.12 ± 0.02 ppm, 0.40 ± 0.05 ppm for length and north, east, and vertical components, respectively. This means that the standard deviations range from 6 to 10 mm for length, 6 to 11 mm for the north component, 7 to 16 mm for the east component, 25 to 54 mm for the vertical component for baseline lengths in the range of 3 to 120 km.

Since the daily baseline solutions of permanent or semi-permanent stations are solved from 24-h continuous GPS data, the precisions of baseline length and components are much better than those for the

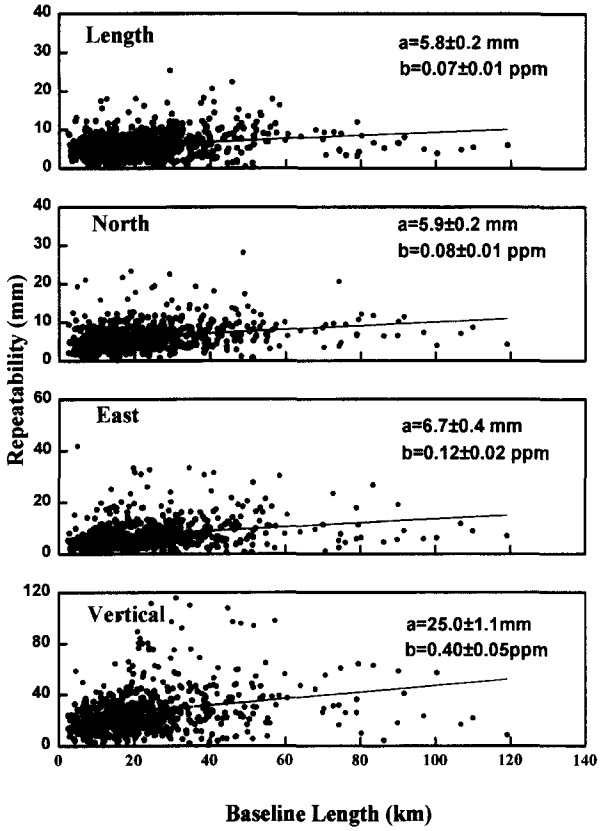

Fig. 3. Long-term repeatability for annually surveyed baselines in the Taiwan GPS Network. Curves are best fits (Eq. 1) through each component.

annually surveyed data. It gives standard deviations in the ranges of 5–10 mm, 5–7 mm, 7–14 mm and 19–33 mm for the length and north, east and vertical components with baseline lengths from 10 to 400 km. It is obvious that the baseline length has the best precision, while the vertical component is the worst. As a consequence, the following discussion, is solely based on the changes in the baseline length from the repeated surveys and continuous GPS data.

4. Changes in baseline length

The observed lengths of each baseline from daily solutions of continuous GPS data, or from the average of observations within 30 days for annually surveyed data, are plotted as a function of time in Fig. 4 and Figs. 6–13. A straight line is fitted to each of the data sets, and the slope of this line gives an estimate of the average rate of length changes. The standard errors of the average rates are also estimated based on the residuals to the best linear fittings. The positive value of length rate denotes an extension, while the negative rate of length change denotes a shortening.

Fig. 4 gives examples of length changes for three baselines between permanent or semi-permanent stations with different rates and lengths. The shortest baseline S104–S105 with a length of only 16 km obviously has the greatest precision as revealed by the smallest scattering. The longest one is from Paisha, Penghu (S01R) to Lanhsu (S102) with a length of about 269 km which covers the whole width of the Taiwan GPS Network (Fig. 2). This baseline (trending 312°) is approximately parallel to the direction of the plate convergence (309°) estimated by Seno et al. (1993) and shows the highest rate of shortening in the network, 82.5 ± 0.3 mm/yr.

The baseline S104–S105 is oblique to the strike of

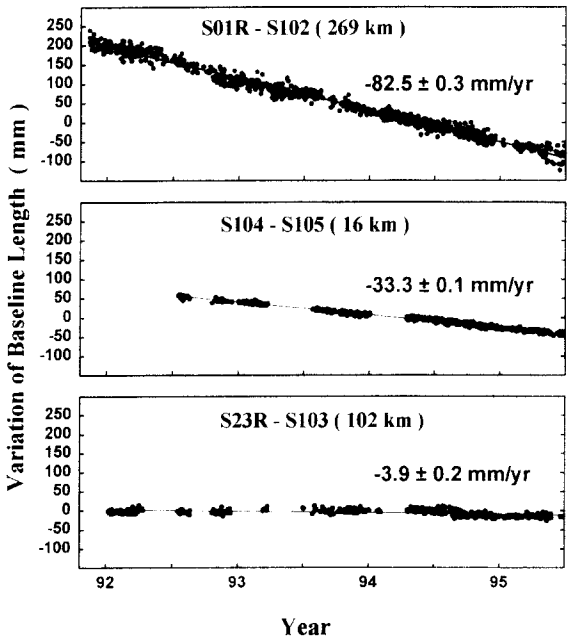

Fig. 4. Time variation plots of length for the three baselines S01R–S102, S104–S105 and S23R–S103 from November 1991 to June 1995. The straight line in each plot is the best linear fitting.

the Longitudinal Valley with an azimuth of 331° (see Fig. 2). It traverses the LVF with one end, Fushan (S104), at the southern tip of the Coastal Range, and with the other, Mingyeh (S105), at the eastern margin of the Central Range. The shortening rate of this baseline, 33.3 ± 0.1 mm/yr, is consistent with that deduced from earlier trilateration data (e.g. Yu et al., 1990, 1992). It has been verified that this extremely high rate of deformation was caused by the aseismic slip on the LVF (Yu and Liu, 1989). The third baseline, S23R–S103, with the intermediate length of 102 km gives a small shortening rate of 3.9 ± 0.2 mm/yr.

All of the three baselines in Fig. 4 and other baselines between permanent or semi-permanent stations show quite linear variations in baseline length. Several moderate earthquakes with magnitudes of more than 5.0 did occur in the Taiwan region during the observation period. However, it seems that they had no significant effect on the length changes of these baselines. Thus, it is reasonable to assume that there was steady motion between the GPS stations during the five-year period of this study. In the following sections, the changes in the baseline length in several distinct geologic provinces are discussed.

4.1. Longitudinal Valley

The length changes of six baselines obliquely traversing the Longitudinal Valley with azimuths from 289° to 354° (Fig. 5) are presented along the strike of the LVF in Fig. 6. The baselines S076–S048 and 1215–0131 were disturbed by the Hualien earthquake sequence of December 1990 (M_L = 6.5, 6.7). Thus, the 1990 data are not included in the estimation of the length rates. It is clear that the baselines to the south of Chihshang (near station 0054 in Fig. 5) have higher shortening rates of 27.5–31.0 mm/yr and the shortening rates decrease toward the north. In fact, in the northernmost baseline 1215–0131, the rate is only 7.2 ± 1.2 mm/yr.

4.2. Coastal Range

Figs. 7–9 illustrate the length changes of eleven baselines in the Coastal Range and five others between Lutao, the volcanic islet offshore southeastern Taiwan, and the stations along the eastern coast of Taiwan (Fig. 5). The horizontal deformation in the southern Coastal Range is not significant (Fig. 7, baselines S054–S072 and S057–S056). It increases toward the northern Coastal Range. The shortening rate is 12.5 ± 1.5 mm/yr on baseline S061–S075. The 1990 data point was also affected by the December 1990 earthquake and is excluded in the rate estimation.

Two baselines oblique to the trend of the Coastal Range, S059–S076 and S077–S074, show very high shortening rates of 36.6 ± 1.6 mm/yr and 33.0 ± 3.7 mm/yr, respectively (see Figs. 5 and 8), comparable to those across the LVF. Another two baselines directed from Fengping (S077) to the north (S077–S061) and the west (S077–S076) also give significant shortening rates of 16.4 and 16.8 mm/yr, respectively. In contrast, two baselines, S059–S077 and S058–S059, to the south of Fengping and more or less in a N–S direction have no detectable deformation. The extraordinary high shortening rates observed on the baselines directed to the west, northwest and north from Fengping may be due to the active reverse faulting there. This fact supports the idea that there may be southward migration of the NW-vergent thrusting of the

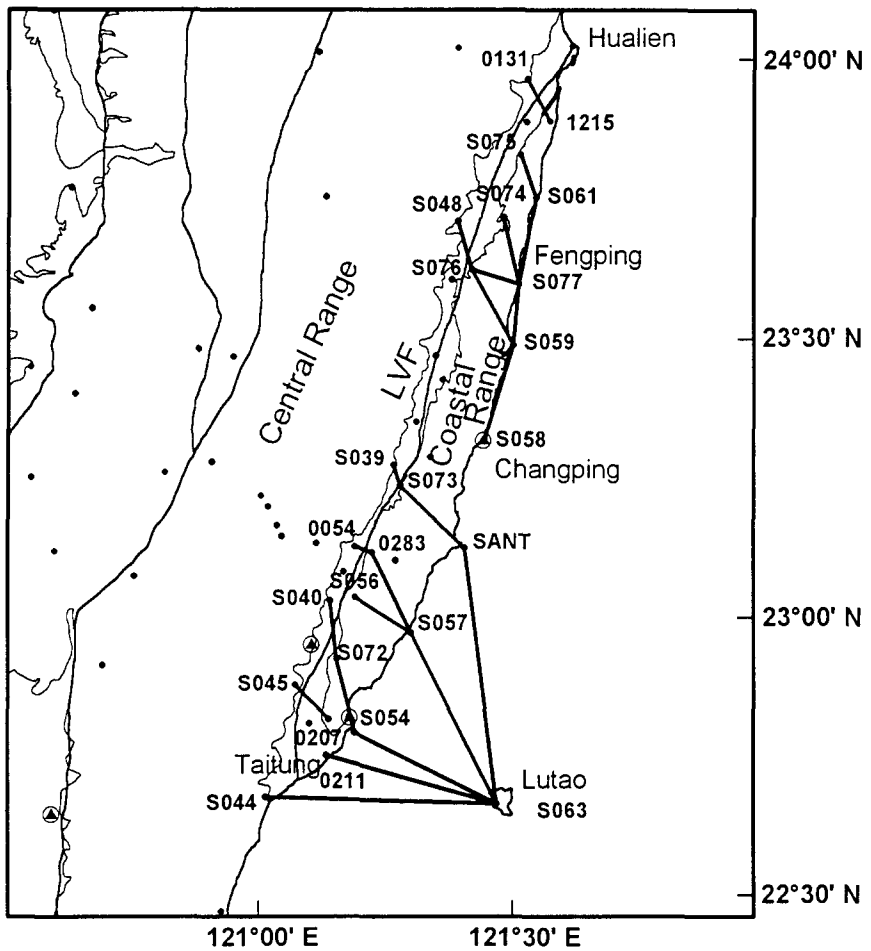

Fig. 5. GPS stations and baselines in the Longitudinal Valley and Coastal Range.

Coastal Range as proposed by Angelier et al. (1995), who also suggested that the NW-vergent thrust motion has been transferred from the LVF (the active thrust to the south) to the NE–SW-trending thrusts obliquely cutting the northern Coastal Range.

Three baselines (S063–S054, S063–S057 and S063–SANT) connecting Lutao with three stations in the southern Coastal Range show a shortening rate of 7–10 mm/yr (Fig. 9). This implies a moderate deformation of the Luzon arc near the plate boundary. The baselines from Lutao to the limestone hill (0211) inside the southern end of the Longitudinal Valley and to the southeastern margin of the Central Range (S044) give shortening rates of 30.8 ± 1.7 mm/yr and 32.3 ± 2.6 mm/yr, respectively. These high rates are undoubtedly due to the slip on the southward extension of the LVF, further supporting the conclusion by Yu et al. (1992) that the surface trace of the LVF is located along the Pinantahsi River which runs more or less along the western margin of the Coastal Range in the southern Longitudinal Valley.

4.3. Southern Central Range and northern Taiwan

Fig. 10 shows the changes of length for six baselines across the southern Central Range with azimuths from 242° to 309° (see Fig. 2). These baselines have remarkable extension rates of 11–27 mm/yr. This extensional deformation is probably due to the oblique convergence and the indentation by the wedge-shaped backstop in eastern Taiwan (Lu and Malavieille, 1994). In northern Taiwan and in

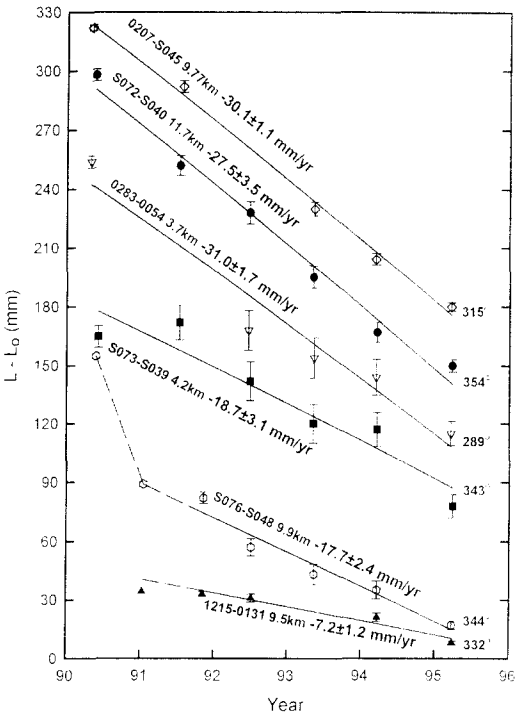

Fig. 6. The observed length L (less a nominal length Lo) plotted as a function of time from 1990 to 1995 for six baselines across the Longitudinal Valley. The straight lines are the best linear fittings. The station names, length, average length rate and azimuth for each baseline are also shown.

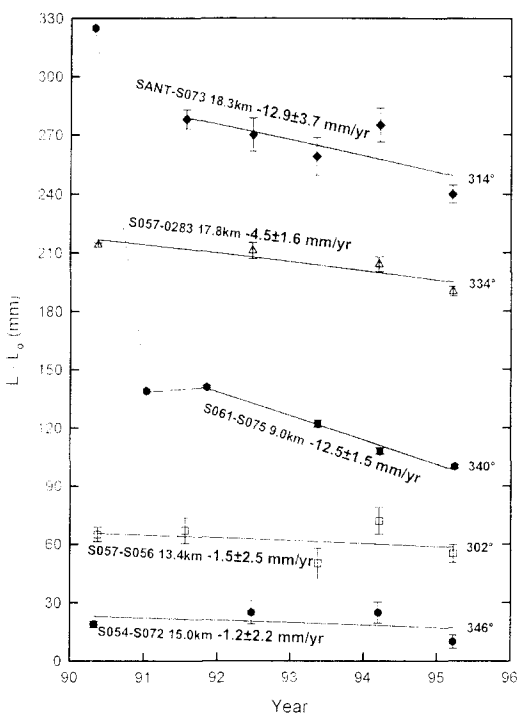

Fig. 7. Same as Fig. 6, except for five baselines in the Coastal Range.

the Ilan area, slight to moderate extension rates of 2–16 mm/yr are observed as shown in Fig. 11. The structural trends of the Taiwan mountain belt bend toward the east-northeast in this area (see Fig. 1b).

4.4. Fold and thrust belt

Thirteen station pairs which constitute thirteen baselines crossing the major thrust faults in central and southern Taiwan have azimuths between 263° and 341° (see Fig. 2). Fig. 12 shows the changes in length for six baselines in central Taiwan, where slight to moderate shortening rates of 3.9–12.7 mm/yr are observed. Fig. 13 illustrates the variation of length for seven baselines across the Chukou Fault in southern Taiwan. Two baselines (S014–S070 and S013–S069) with lengths of about 10 km give slight contraction rates of 4.6–5.0 mm/yr. The other five baselines indicate remarkable shortening rates of 11.0–27.9 mm/yr. The rates seem to more

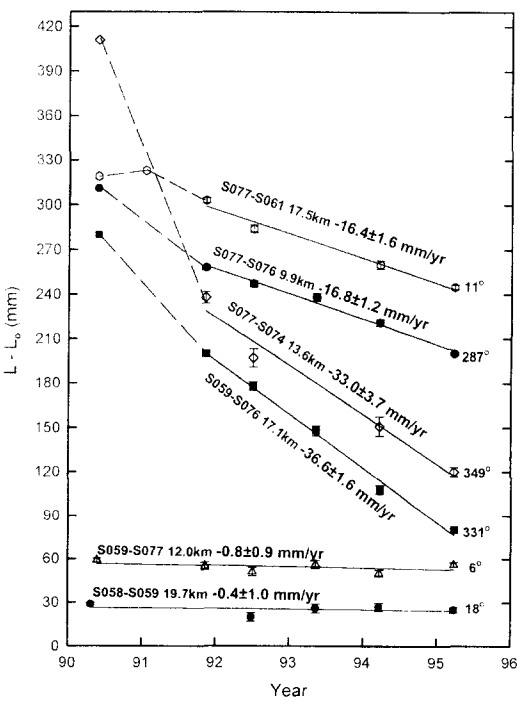

Fig. 8. Same as Fig. 6, except for six baselines near Fengping (S077).

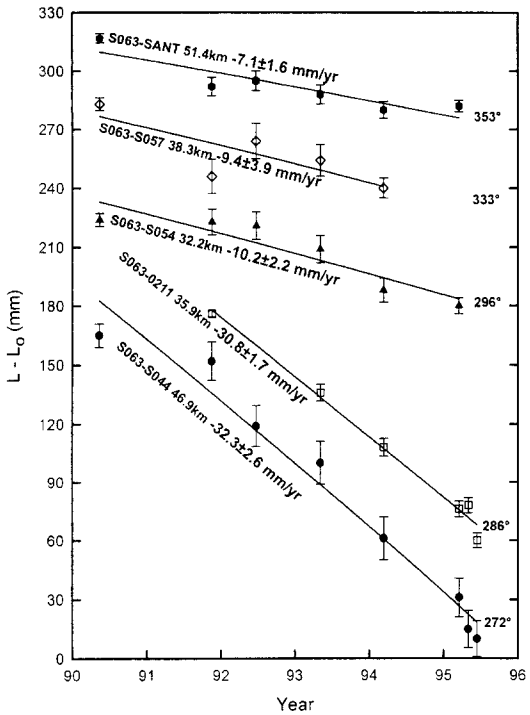

Fig. 9. Same as Fig. 6, except for five baselines directed from Lutao (S063).

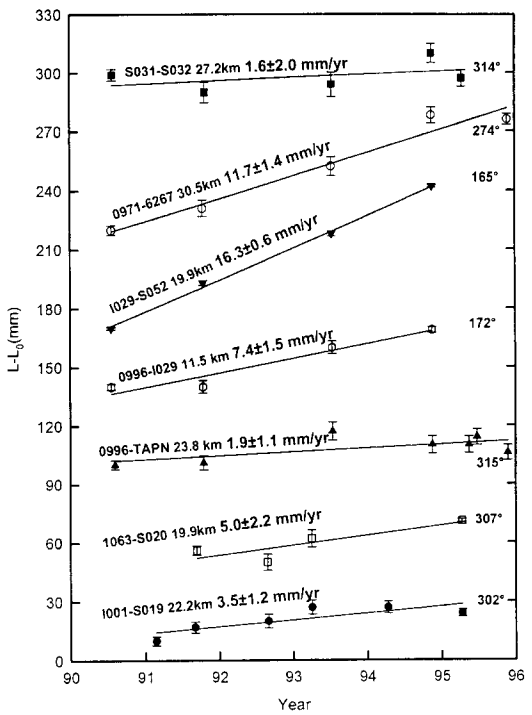

Fig. 11. Same as Fig. 6, except for seven baselines in northern Taiwan and the Ilan area.

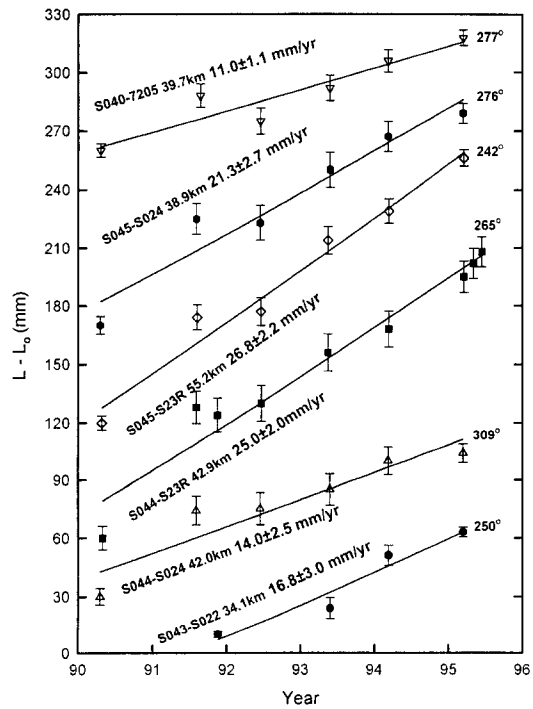

Fig. 10. Same as Fig. 6, except for six baselines across the southern Central Range.

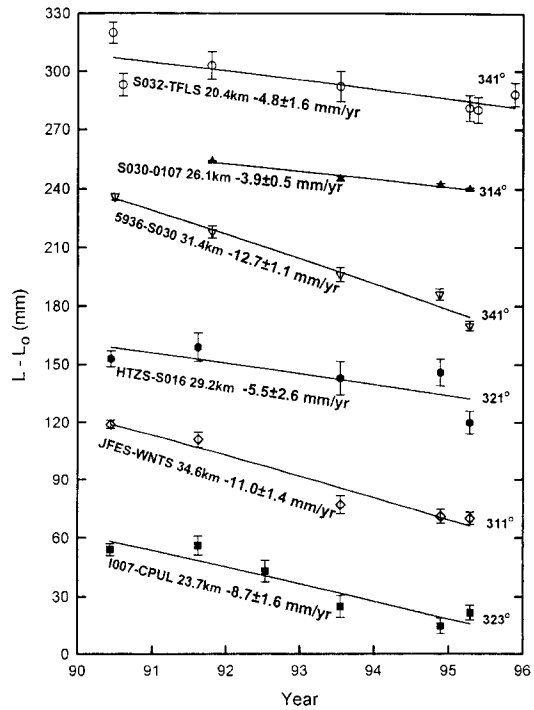

Fig. 12. Same as Fig. 6, except for six baselines in central Taiwan.

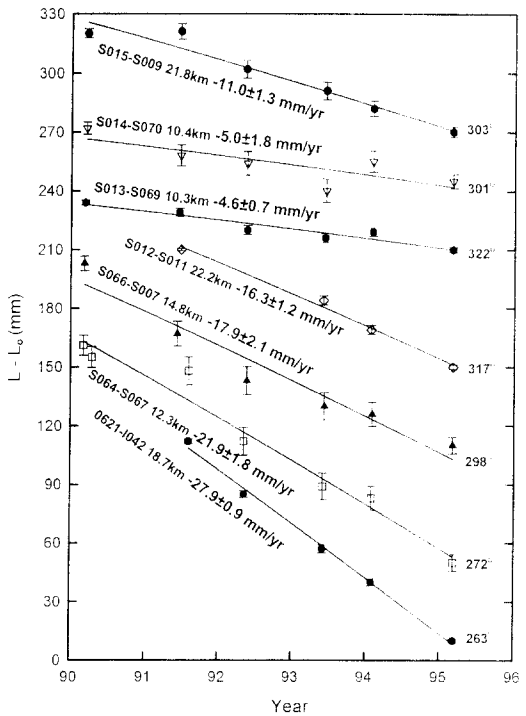

Fig. 13. Same as Fig. 6, except for seven baselines across the Chukou fault.

or less depend on the baseline length, implying that the deformation is likely to be distributed in a wide zone and not solely to be caused by the slip along the faults. In other words, the crustal strain probably accumulates in this area. The results of GPS observation on the densified profiles across the faults may clarify this inference. In general, the shortening rates along the strike of the Chukou Fault (Fig. 2) increase toward the south, and near the southern end of the fault extremely high rates of 21.9 ± 1.8 mm/yr and 27.9 ± 0.9 mm/yr are detected.

5. Velocity field

The average rates of length change on each baseline between nearby stations, which are usually observed in the same session, are determined by linear regression in time. In total, the rates of 522 baselines from annual surveys and 26 baselines based on the continuous GPS data are estimated.

During the period of November 1991 to June 1995, the average rates of change on the north and east components of the baseline between the two permanent GPS stations at Paisha, Penghu (S01R) and Taipei (T986) are only 0.3 ± 0.2 mm/yr and 1.6 ± 0.4 mm/yr, respectively. This means that the relative horizontal motion between these two stations may be negligible. Thus in the calculation of station velocities, the Paisha station (S01R) situated at the relatively stable Chinese continental margin is chosen as the fixed station, and the azimuth from Paisha to Taipei (52.1°) is fixed. This procedure is necessary for resolving the translational and rotational ambiguities of the whole network in the estimation which follows.

The individual values of the average length rate from the 548 baselines in the Taiwan GPS Network are weighted by the reciprocal square of the standard error in the rate. These weighted rates are then used in a least-squares adjustment to estimate the station velocities relative to the fixed station S01R (Prescott, 1981). Tables 1 and 2 give the geographic coordinates, the estimated relative velocities and pertinent data of 22 stations in the Coastal Range and 118 stations in the remaining part of Taiwan, respectively. V_E and V_N represent the east and north components with positive values representing the eastward and northward motions, respectively. V is the magnitude of the resultant velocity vector. The azimuth of the vector is measured clockwise from the north. This velocity field of the GPS stations in the Taiwan area is shown in Fig. 14. The 95% confidence ellipse is also indicated at the tip of each velocity vector.

The velocities of stations in the Coastal Range are in the directions of 295°–348° (see Table 1 and Fig. 14). The moving rates to the south of Fengping (S077) range from 56 to 70 mm/yr. In contrast, there is a dramatic decrease in the rates (11–40 mm/yr) to the north of Fengping. As mentioned in the previous section, this may be due to the active thrust motion crossing the Coastal Range. The station at Lutao (S063) has a velocity of 78.3 ± 1.7 mm/yr in 312° ± 2°, the same as that reported by Yu and Chen (1994). On the other hand, the permanent station at Lanhsu (S102) gives a velocity of 81.5 ± 1.3 mm/yr in 306° ± 1°, with the moving rate about 5 mm/yr less than that in the previous report. However, the uncertainty of the estimation in this study is also smaller. Whether this is caused by the short-term variation in plate motion or just by an

Table 1
Velocities of GPS stations in the Coastal Range

Station	Lat. (°)	Long. (°)	V_E (mm/yr)	V_N (mm/yr)	V (mm/yr)	Azimuth (°)
1215	23.8896	121.5787	−9.3 ± 3.0	13.9 ± 2.1	16.7 ± 2.4	326.2 ± 2.8
S075	23.8294	121.5203	−6.2 ± 5.5	9.6 ± 2.5	11.4 ± 3.6	327.1 ± 4.8
S061	23.7528	121.5506	−5.0 ± 4.3	23.3 ± 2.2	23.8 ± 2.3	347.9 ± 4.2
S074	23.7177	121.4871	−10.7 ± 3.7	18.6 ± 3.0	21.5 ± 3.2	330.1 ± 3.5
S076	23.6252	121.4242	−36.0 ± 3.5	16.5 ± 2.2	39.6 ± 3.3	294.6 ± 2.5
S077	23.5982	121.5169	−43.4 ± 3.8	49.3 ± 1.9	65.7 ± 2.9	318.6 ± 3.1
S059	23.4902	121.5052	−47.2 ± 3.2	51.4 ± 1.7	69.8 ± 2.5	317.4 ± 2.6
S058	23.3212	121.4463	−40.0 ± 0.9	50.5 ± 0.9	64.4 ± 0.9	321.6 ± 0.9
1047	23.4302	121.3651	−44.6 ± 3.2	35.6 ± 2.1	57.1 ± 2.8	308.6 ± 2.6
0135	23.2925	121.3404	−36.5 ± 2.6	43.0 ± 1.9	56.4 ± 2.2	319.7 ± 2.3
S073	23.2415	121.2800	−44.4 ± 2.6	36.5 ± 2.2	57.5 ± 2.4	309.4 ± 2.4
SANT	23.1269	121.4083	−47.9 ± 2.2	47.7 ± 1.7	67.6 ± 2.0	314.9 ± 2.0
0283	23.1196	121.2254	−45.2 ± 2.2	46.6 ± 2.0	64.9 ± 2.1	315.9 ± 2.1
S033	23.1048	121.2718	−46.3 ± 2.4	47.5 ± 2.3	66.3 ± 2.3	315.7 ± 2.4
S056	23.0387	121.1904	−45.8 ± 1.9	41.8 ± 2.0	62.0 ± 1.9	312.4 ± 2.0
S057	22.9748	121.3012	−46.9 ± 1.9	48.8 ± 1.6	67.7 ± 1.8	316.1 ± 1.8
S072	22.9274	121.1545	−49.2 ± 1.7	40.8 ± 1.6	63.9 ± 1.7	309.7 ± 1.6
0207	22.8197	121.1395	−45.9 ± 1.3	37.2 ± 1.6	59.1 ± 1.4	309.0 ± 1.5
S104	22.8226	121.1813	−47.0 ± 1.0	43.0 ± 1.1	63.7 ± 1.0	312.5 ± 1.1
S054	22.7958	121.1894	−47.8 ± 1.6	44.8 ± 1.8	65.5 ± 1.7	313.1 ± 1.7
S063	22.6664	121.4704	−58.4 ± 1.7	52.1 ± 1.8	78.3 ± 1.7	311.7 ± 1.8
S102	22.0354	121.5490	−65.7 ± 1.4	48.3 ± 1.0	81.5 ± 1.3	306.3 ± 1.2

Note: V_E is east component, V_N is north component, $V = (V_E^2 + V_N^2)^{1/2}$.

observation error still needs further clarification. The GPS observed moving direction of Lanhsu relative to Paisha is 306°, which is essentially the same as the direction of relative motion (309°) between the Philippine Sea plate (PH) and the Eurasian plate (EU) near Taiwan, as estimated by Seno (1977) and Seno et al. (1993). Nevertheless, in either case, the rate is about 15% faster than the plate convergence suggested previously. This result implies that there may be significant extensional deformations between Penghu Islands and the stable Asian continent or to the east of the volcanic islets of Lutao and Lanhsu. An alternative interpretation is that Seno's estimation of the PH-EU's Euler-pole and rotational velocity may need to be corrected. When the geologic process due to the arc–continent collision is considered, the GPS observed velocity of Lanhsu (arc) relative to Penghu (continental margin) can better be used.

After passing the Longitudinal Valley, there is a major discontinuity of about 30 mm/yr in station velocity, and the moving direction shifts from NW in the Coastal Range to WNW in the eastern margin of the Central Range. The orientation of the station velocities in the Western Foothills is almost always to the west. Very rapid station velocities of 41–49 mm/yr in the west to southwest direction are observed in the Kaohsiung–Pingtung area. This may be explained by the escaping of this area to the weak accretionary wedge offshore southwestern Taiwan as the indentation and oblique convergence go on in eastern Taiwan.

Another velocity discontinuity of 10–28 mm/yr is detected across the Chukou Fault where remarkable strain accumulation rates are also observed (Yu and Chen, 1994). Station velocities in the Coastal Plain and central Taiwan are mostly only marginally significant to insignificant. To the north of the Peikang High, the velocities gradually change direction from west to north, and finally to east or southeast in the Ilan area. Slight extensional crustal motion in the NW–SE direction is found in northern Taiwan and the Ilan Plain, obviously related to the back-arc extension of the Okinawa trough (Kimura, 1985).

The velocity field in the fold and thrust belt of western Taiwan generally shows a fan-shaped pattern, which is consistent with the directions of max-

Table 2
Velocities of GPS stations in the Taiwan area

Station	Lat. (°)	Long. (°)	V_E (mm/yr)	V_N (mm/yr)	V (mm/yr)	Azimuth (°)
0054	23.1305	121.1909	−23.6 ± 2.3	19.9 ± 2.1	30.9 ± 2.2	310.1 ± 2.2
0107	24.4461	120.8361	−0.2 ± 2.3	−2.2 ± 1.9	2.2 ± 1.9	185.2 ± 2.3
0131	23.9655	121.5349	−2.1 ± 2.6	9.2 ± 2.1	9.4 ± 2.1	347.1 ± 2.6
0201	23.3558	121.3119	−19.0 ± 4.3	21.9 ± 2.1	29.0 ± 3.2	319.1 ± 3.5
0206	22.8118	121.1012	−42.0 ± 1.4	13.3 ± 1.5	44.1 ± 1.4	287.6 ± 1.5
0211	22.7553	121.1340	−36.6 ± 1.7	16.7 ± 1.6	40.2 ± 1.7	294.5 ± 1.6
0216	24.0246	121.6227	2.9 ± 3.3	6.9 ± 2.5	7.5 ± 2.6	22.8 ± 3.2
0505	24.7482	121.7489	6.3 ± 2.0	−1.1 ± 1.9	6.4 ± 2.0	99.9 ± 1.9
0621	22.7915	120.4258	−45.6 ± 1.4	−7.8 ± 1.5	46.3 ± 1.4	260.3 ± 1.5
0727	23.6074	121.3843	−27.1 ± 3.2	11.2 ± 2.1	29.3 ± 3.1	292.5 ± 2.3
0801	25.2140	121.4852	−4.2 ± 2.2	−1.8 ± 1.6	4.6 ± 2.1	246.8 ± 1.7
0971	24.6651	121.6877	11.5 ± 2.6	7.1 ± 2.3	13.5 ± 2.5	58.3 ± 2.4
0980	24.8905	121.1632	−1.2 ± 2.5	−2.6 ± 4.9	2.9 ± 4.6	204.8 ± 3.1
0982	25.1152	121.4492	−7.5 ± 1.7	−1.7 ± 1.6	7.7 ± 1.7	257.2 ± 1.6
0991	25.0185	121.3224	−5.8 ± 1.6	0.5 ± 2.4	5.8 ± 1.6	274.9 ± 2.4
0996	24.8722	121.7935	0.3 ± 1.5	−0.6 ± 1.9	0.7 ± 1.8	153.4 ± 1.6
1043	24.9943	121.5404	1.4 ± 1.1	−0.9 ± 1.1	1.7 ± 1.1	122.7 ± 1.1
1045	25.1309	121.5992	−2.4 ± 1.6	0.5 ± 1.3	2.5 ± 1.6	281.8 ± 1.3
1055	25.1107	121.6910	−2.5 ± 1.9	1.8 ± 2.3	3.1 ± 2.0	305.8 ± 2.2
1063	25.1792	121.6617	−3.1 ± 1.9	2.1 ± 1.9	3.7 ± 1.9	235.9 ± 1.9
1064	25.0861	121.5211	−4.5 ± 1.5	−1.8 ± 2.3	4.8 ± 1.6	248.2 ± 2.2
1119	25.2546	121.5957	−2.9 ± 2.6	1.8 ± 1.8	3.4 ± 2.4	301.8 ± 2.1
1168	25.1449	121.7674	−3.0 ± 1.6	3.3 ± 2.5	4.5 ± 2.1	317.7 ± 2.1
1449	24.0221	121.3962	3.0 ± 2.5	12.0 ± 3.4	12.4 ± 3.4	14.0 ± 2.6
S121	24.8525	121.2416	0.5 ± 1.8	4.3 ± 2.2	4.3 ± 2.2	6.6 ± 1.8
5936	24.0147	121.1186	−9.3 ± 1.9	13.4 ± 1.8	16.3 ± 1.8	325.2 ± 1.9
6267	24.6863	121.3870	−1.5 ± 2.1	3.5 ± 1.6	3.8 ± 1.7	336.8 ± 2.0
6389	24.1542	121.2764	−1.7 ± 2.0	19.4 ± 1.9	19.5 ± 1.9	355.0 ± 2.0
7205	23.0768	120.7574	−40.5 ± 1.5	4.0 ± 1.2	40.7 ± 1.5	275.6 ± 1.2
8046	23.0843	121.1684	−31.1 ± 3.0	22.4 ± 2.0	38.3 ± 2.7	305.8 ± 2.4
A247	24.0222	120.3996	0.5 ± 2.1	1.5 ± 2.0	1.6 ± 2.0	18.4 ± 2.1
CHSN	25.1725	121.5452	−6.3 ± 2.0	3.8 ± 1.8	7.4 ± 1.9	301.1 ± 1.9
CKLS	25.0948	121.8574	−4.2 ± 1.5	3.0 ± 2.6	5.2 ± 1.9	305.5 ± 2.3
CPUL	23.9293	120.6266	−0.9 ± 1.7	2.0 ± 1.8	2.2 ± 1.8	335.8 ± 1.7
HTZS	23.9757	120.9739	−9.1 ± 1.8	7.5 ± 1.7	11.8 ± 1.8	309.5 ± 1.7
I001	24.9985	121.4706	−1.3 ± 1.1	0.4 ± 1.6	1.4 ± 1.2	287.1 ± 1.6
I004	22.9753	120.2310	−7.6 ± 1.7	−2.7 ± 1.4	8.1 ± 1.7	250.4 ± 1.4
I007	23.7580	120.7663	−8.9 ± 1.8	9.9 ± 1.6	13.3 ± 1.7	318.0 ± 1.7
I029	24.7696	121.8084	10.7 ± 2.1	−7.7 ± 2.1	13.2 ± 2.1	125.7 ± 2.1
I042	22.7718	120.2446	−17.9 ± 1.6	−2.1 ± 1.6	18.0 ± 1.6	263.3 ± 1.6
I045	22.6694	120.3194	−42.4 ± 1.8	−21.2 ± 1.6	47.4 ± 1.8	243.4 ± 1.6
I301	24.6857	121.7633	14.1 ± 2.8	−2.2 ± 2.1	14.3 ± 2.8	98.9 ± 2.1
JFES	23.9363	120.8335	−5.9 ± 2.0	9.7 ± 2.1	11.4 ± 2.1	328.7 ± 2.0
KLUN	24.9976	121.3760	−3.8 ± 1.0	0.0 ± 1.6	3.8 ± 1.0	270.0 ± 1.6
KUYN	25.0392	121.0679	−0.4 ± 1.9	−2.4 ± 4.1	2.4 ± 4.1	189.5 ± 2.0
LIUC	22.3427	120.3707	−41.9 ± 2.9	−14.7 ± 3.2	44.4 ± 2.9	250.7 ± 3.2
MERK	23.7991	120.3012	0.8 ± 1.3	2.8 ± 1.7	2.9 ± 1.7	15.9 ± 1.3
P049	25.1674	121.5727	−1.1 ± 2.1	−1.0 ± 1.3	1.5 ± 1.8	227.7 ± 1.7
S002	23.2151	119.4304	5.2 ± 1.3	2.9 ± 1.9	6.0 ± 1.5	60.9 ± 1.8
S003	23.1749	120.1546	1.0 ± 1.4	1.1 ± 1.5	1.5 ± 1.5	42.3 ± 1.4
S004	23.3842	120.1806	1.3 ± 1.4	4.6 ± 1.5	4.8 ± 1.5	15.8 ± 1.4
S005	23.6009	120.2085	0.2 ± 1.7	1.8 ± 1.9	1.8 ± 1.9	6.3 ± 1.7
S006	23.5981	120.3547	−4.0 ± 1.8	2.6 ± 1.8	4.8 ± 1.8	303.0 ± 1.8

Table 2 (continued)

Station	Lat. (°)	Long. (°)	V_E (mm/yr)	V_N (mm/yr)	V (mm/yr)	Azimuth (°)
S007	23.2559	120.3751	−10.4 ± 1.5	4.6 ± 1.8	11.4 ± 1.6	293.9 ± 1.8
S008	23.4218	120.4355	−7.6 ± 1.9	4.6 ± 1.7	8.9 ± 1.8	301.2 ± 1.8
S009	23.6624	120.4934	−2.7 ± 1.8	8.3 ± 2.0	8.7 ± 2.0	342.0 ± 1.8
S010	22.5254	120.3718	−37.3 ± 2.9	−17.1 ± 2.0	41.0 ± 2.8	245.4 ± 2.2
S011	23.2072	120.3314	−5.1 ± 1.5	3.2 ± 1.6	6.0 ± 1.5	302.1 ± 1.6
S012	23.0612	120.4802	−30.5 ± 1.7	1.8 ± 1.5	30.6 ± 1.7	273.4 ± 1.5
S013	23.2554	120.5556	−23.6 ± 1.6	8.6 ± 1.4	25.1 ± 1.6	290.0 ± 1.4
S014	23.4062	120.6406	−21.1 ± 1.7	9.2 ± 1.5	23.0 ± 1.7	293.6 ± 1.5
S015	23.5568	120.6733	−15.5 ± 1.8	8.3 ± 1.6	17.6 ± 1.8	298.2 ± 1.6
S016	24.1813	120.7947	−4.1 ± 2.0	4.9 ± 1.8	6.4 ± 1.9	320.1 ± 1.9
S017	24.6030	120.7563	1.6 ± 2.0	−3.2 ± 2.0	3.6 ± 2.0	153.4 ± 2.0
S018	24.8850	120.9919	−2.4 ± 1.6	−5.2 ± 2.1	5.7 ± 2.0	204.8 ± 1.7
S019	25.1039	121.2832	−5.6 ± 1.4	−1.4 ± 2.4	5.8 ± 1.5	256.0 ± 2.4
S020	25.2870	121.5041	−6.6 ± 2.9	0.4 ± 1.8	6.6 ± 2.9	273.5 ± 1.8
S021	21.9969	120.7051	−47.0 ± 3.4	5.0 ± 2.3	47.3 ± 3.4	276.1 ± 2.3
S022	22.3683	120.6157	−48.2 ± 2.2	5.3 ± 2.3	48.5 ± 2.2	276.3 ± 2.3
S024	22.9174	120.6954	−47.6 ± 1.5	2.6 ± 1.3	47.7 ± 1.5	273.1 ± 1.3
S025	23.2654	120.8163	−31.1 ± 2.1	6.4 ± 1.7	31.8 ± 2.1	281.6 ± 1.7
S026	23.2840	120.9082	−31.3 ± 1.9	8.1 ± 1.7	32.3 ± 1.9	284.5 ± 1.7
S027	23.4856	120.8814	−26.7 ± 1.8	9.0 ± 1.6	28.2 ± 1.8	288.6 ± 1.6
S029	25.1289	121.5099	−4.1 ± 1.7	0.5 ± 1.6	4.1 ± 1.7	277.0 ± 1.6
S030	24.2825	121.0193	1.1 ± 2.1	3.9 ± 1.8	4.1 ± 1.8	15.8 ± 2.1
S031	24.3395	121.2999	4.2 ± 2.5	5.1 ± 1.8	6.6 ± 2.1	39.5 ± 2.2
S032	24.5083	121.1058	−2.6 ± 2.1	4.3 ± 1.8	5.0 ± 1.9	328.8 ± 2.0
S035	25.0074	121.9911	−0.6 ± 1.5	1.9 ± 3.2	2.0 ± 3.1	342.5 ± 1.7
S038	23.7554	121.1330	−23.8 ± 2.4	9.8 ± 2.0	25.7 ± 2.3	292.4 ± 2.1
S039	23.2781	121.2677	−19.3 ± 3.6	23.9 ± 2.3	30.7 ± 2.9	321.1 ± 3.2
S040	23.0324	121.1419	−28.6 ± 1.8	17.6 ± 2.0	33.6 ± 1.9	301.6 ± 1.9
S041	21.9280	120.8408	−40.8 ± 2.6	17.3 ± 1.7	44.3 ± 2.5	293.0 ± 1.9
S042	22.2436	120.8468	−39.7 ± 1.6	15.8 ± 1.7	42.7 ± 1.6	291.7 ± 1.7
S043	22.4735	120.9269	−32.9 ± 2.2	14.7 ± 1.9	36.0 ± 2.2	294.1 ± 2.0
S044	22.6796	121.0144	−25.8 ± 1.5	11.0 ± 1.4	28.0 ± 1.5	293.1 ± 1.4
S045	22.8821	121.0724	−25.4 ± 1.4	14.1 ± 1.4	29.1 ± 1.4	299.0 ± 1.4
S046	23.1491	121.0468	−24.7 ± 2.3	17.2 ± 1.9	30.1 ± 2.2	304.9 ± 2.0
S047	23.4725	121.3514	−25.1 ± 2.1	25.4 ± 1.8	35.7 ± 2.0	315.3 ± 2.0
S048	23.7113	121.3970	−17.6 ± 2.6	8.1 ± 2.3	19.4 ± 2.6	294.7 ± 2.4
S049	23.8885	121.5324	−6.2 ± 2.6	7.9 ± 2.0	10.0 ± 2.2	321.9 ± 2.4
S050	24.1470	121.6544	4.1 ± 2.2	2.4 ± 2.2	4.8 ± 2.2	59.7 ± 2.2
S052	24.5957	121.8597	4.9 ± 4.2	−26.0 ± 2.7	26.5 ± 2.8	169.3 ± 4.2
S053	24.3991	121.7698	14.1 ± 4.7	−2.7 ± 4.0	14.4 ± 4.7	100.8 ± 4.0
S055	23.1359	121.1148	−25.6 ± 3.9	18.5 ± 4.8	31.6 ± 4.2	305.9 ± 4.5
S064	22.9504	120.4957	−40.2 ± 1.9	2.9 ± 1.5	40.3 ± 1.9	274.1 ± 1.5
S065	23.1216	120.6029	−33.9 ± 1.7	7.4 ± 1.5	34.7 ± 1.7	282.3 ± 1.5
S066	23.1940	120.5036	−28.6 ± 1.8	6.2 ± 1.5	29.3 ± 1.8	282.2 ± 1.5
S067	22.9531	120.3759	−17.9 ± 1.8	−7.4 ± 2.1	19.4 ± 1.8	247.5 ± 2.1
S069	23.3282	120.4930	−20.8 ± 1.7	5.0 ± 1.6	21.4 ± 1.7	283.5 ± 1.6
S070	23.4538	120.5540	−14.7 ± 2.1	6.2 ± 1.6	16.0 ± 2.0	292.9 ± 1.7
S071	23.4711	120.3139	−4.4 ± 1.7	4.7 ± 1.8	6.4 ± 1.8	316.9 ± 1.7
S078	23.1688	121.0371	−36.3 ± 4.8	3.4 ± 4.7	36.5 ± 4.8	275.4 ± 4.7
S079	23.2028	121.0188	−39.4 ± 6.6	0.3 ± 4.6	39.4 ± 6.6	270.4 ± 4.6
S080	23.2220	121.0050	−31.0 ± 3.9	14.9 ± 4.3	34.4 ± 4.0	295.7 ± 4.2
S101	25.0422	121.6056	0.7 ± 1.0	0.5 ± 1.0	0.9 ± 1.0	54.5 ± 1.0
S103	23.5661	120.4671	−7.3 ± 0.8	2.6 ± 1.0	7.7 ± 0.8	289.6 ± 1.0

Table 2 (continued)

Station	Lat. (°)	Long. (°)	V_E (mm/yr)	V_N (mm/yr)	V (mm/yr)	Azimuth (°)
S105	22.9535	121.1048	29.3 ± 0.9	15.1 ± 1.1	33.0 ± 0.9	297.3 ± 1.1
S23R	22.6468	120.5981	−48.9 ± 0.9	2.4 ± 0.9	49.0 ± 0.9	272.8 ± 0.9
S411	25.1191	121.3925	−5.2 ± 1.7	0.7 ± 1.8	5.2 ± 1.7	277.7 ± 1.8
S412	25.0793	121.4492	0.0 ± 1.4	2.4 ± 1.6	2.4 ± 1.6	0.0 ± 1.4
S413	24.9737	121.5715	−0.5 ± 1.6	−2.3 ± 1.5	2.4 ± 1.5	192.3 ± 1.6
SNHS	24.5110	121.5558	12.5 ± 3.3	6.1 ± 2.3	13.9 ± 3.1	64.0 ± 2.5
STCS	23.5376	120.4726	−8.8 ± 1.7	2.2 ± 1.5	9.1 ± 1.7	284.0 ± 1.5
T986	25.0231	121.5283	0.9 ± 0.7	0.7 ± 0.5	1.1 ± 0.6	52.1 ± 0.6
TAPN	25.0249	121.6273	1.0 ± 1.0	0.1 ± 1.4	1.0 ± 1.0	275.7 ± 1.4
TECS	24.3581	120.6469	−10.5 ± 3.4	2.5 ± 2.2	10.8 ± 3.3	283.4 ± 2.3
TFLS	24.6822	121.0418	1.9 ± 2.0	0.3 ± 2.1	1.9 ± 2.0	81.0 ± 2.1
WNTS	24.1399	120.5763	0.1 ± 1.9	−0.2 ± 1.7	0.2 ± 1.7	206.6 ± 1.9

Note: V_E is east component, V_N is north component, $V = (V_E^2 + V_N^2)^{1/2}$.

imum compressional tectonic stress inferred from the earthquake focal mechanisms (Yeh et al., 1991), borehole breakout data (Suppe et al., 1985), and Quaternary fault slip data (Angelier et al., 1986, 1990). Based on the GPS data of Yu and Chen (1994), Hu et al. (1995) employed a 2-D distinct-element numerical model to evaluate the influences on the active deformation of southern Taiwan. They concluded that the active velocity field in southwestern Taiwan strongly depends on (1) the presence and shape of the Peikang High, (2) the presence of major active discontinuities (the LVF and the major thrusts of western Taiwan), and (3) the neighbouring weakness zone of the accretionary prism of the northern Manila subduction zone. To interpret the pattern of the velocity field in the whole of Taiwan, a much more complicated 3-D numerical model is required.

6. Conclusion

The Taiwan GPS Network is composed of 131 annually surveyed mobile stations and 9 permanent or semi-permanent continuously recording stations. The mobile stations were surveyed 4–6 times from March 1990 to November 1995, while the earliest established continuous GPS stations have been operated since November 1991. In this study, both the epoch measurements and the continuous GPS data are processed with Bernese GPS software v.3.4, using the available precise ephemerides provided by the SIO or IGS. The changes in baseline length obtained from the repeated surveys and continuous data are utilized to study the crustal deformation and to estimate the relative velocities of the GPS stations in the Taiwan area. The findings are summarized here:

(1) With an observation session of 6–14 h, the standard deviations of the annually surveyed baseline lengths during the period of this study are in the range of 6–10 mm for baselines from 3 to 120 km.

(2) Daily solutions of continuous GPS stations are solved using 24-h data, which affords a better precision for baseline length. The standard deviations are 5–10 mm for baselines in the range of 10 to 400 km.

(3) As demonstrated by the quite uniform variations of baseline length, as determined from the continuous GPS data, it is reasonable to assume steady motion between most of the GPS stations during the five-year period of this study when estimating the average rates of length change.

(4) The extraordinarily high shortening rates of 16–36 mm/yr on the baselines directed to the west, northwest and north from Fengping indicate that the NE–SW-trending thrusts obliquely cutting the northern Coastal Range may indeed be very active.

(5) The baselines traversing the Longitudinal Valley to the south of Chihshang yield shortening rates of 27.5–31.0 mm/yr, which are in good agreement with those observed previously in repeated trilateration surveys (Yu et al., 1990, 1992).

(6) Remarkable extension rates of 11–27 mm/yr are observed for the baselines across the southern Central Range, while slight to moderate extension rates which must be related to the back arc extension

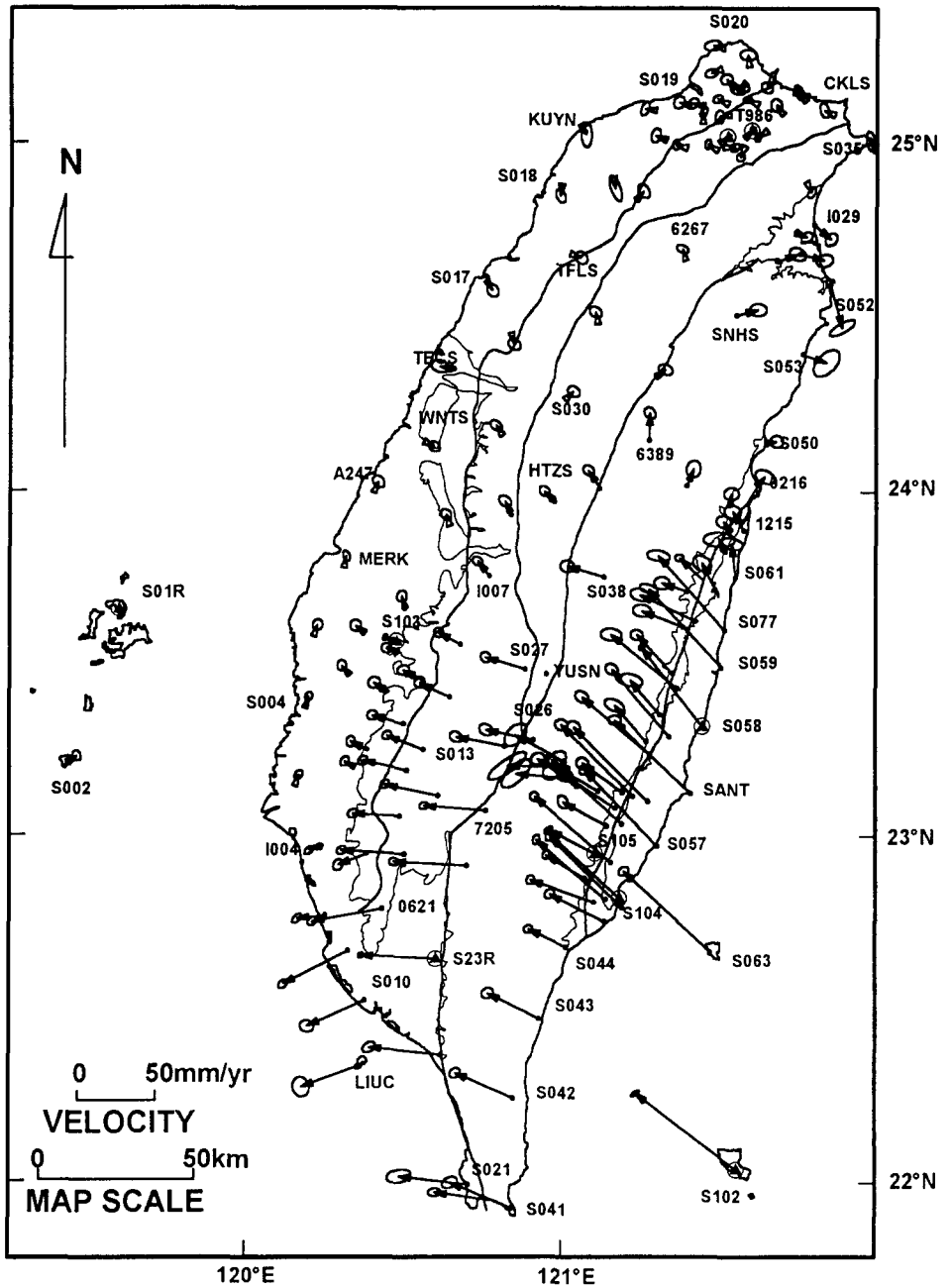

Fig. 14. Velocities of GPS stations relative to Paisha, Penghu (S01R). The 95% confidence ellipse is shown at the tip of each velocity vector.

of the Okinawa trough are also detected in the Ilan area and northern Taiwan.

(7) Based on the dependence of the shortening rate on the baseline length and the higher rates compared with those in the adjacent area, the crustal strain is likely to be accumulating significantly in the vicinity of the Chukou Fault. For this, observations in this area clearly need to be intensified.

(8) The velocities of stations in the Coastal Range are in the directions of 295°–348°. The moving rates

to the south of Fengping range from 56–70 mm/yr. On the other hand, there is a dramatic decrease in the rates (11–40 mm/yr) to the north of Fengping.

(9) The GPS observed moving direction of Lanhsu (Luzon arc) relative to Paisha (Chinese continental margin) is 306° ± 1°, which is essentially the same as the direction of plate convergence (309°) (Seno, 1977; Seno et al., 1993). However, the rate of 81.5 ± 1.3 mm/yr is about 15% faster than that of the relative motion between the Philippine Sea plate and Eurasian plate. This difference in the rates may be a result of the significant southeastward movement of Paisha relative to the stable Asian continent. An alternative is that Seno's estimation of the PH-EU's Euler-pole and rotational velocity need to be further refined.

(10) Two major discontinuities of about 30 mm/yr and 10–28 mm/yr are detected across the LVF and the Chukou Fault, respectively.

(11) In the fold and thrust belt of western Taiwan, the velocity field shows a fan-shaped pattern which is consistent with the directions of present-day and Quaternary tectonic stress. The presence and shape of the Peikang High, the major thrusts and the weak zone of the accretionary wedge offshore southwestern Taiwan have much influence on the active deformation pattern of this area.

(12) The station velocities in the Coastal Plain, central Taiwan and northern Taiwan are mostly only marginal or not significant. A few more years of GPS observation are required for the crustal motion in the area to be accurately determined.

Acknowledgements

The authors would like to express their sincere thanks to many of their colleagues and part-time assistants who have devoted their efforts to the GPS field surveys and the collection of the continuous GPS data during the past few years. They are indebted to Prof. Y. Bock of Scripps Institution of Oceanography (SIO), San Diego, U.S.A., and all the participants of the International GPS Service for Geodynamics (IGS) who have provided the precise ephemerides for data processing. Gratitude is also extended to Prof. G. Beutler and his colleagues for generously supporting the updated versions of the Bernese GPS software. Appreciation is also due to Mr. Y.H. Lee of the Ministry of Interior, R.O.C., who provided part of the 1995 epoch survey data in this study, and to our colleagues Miss S.H. Wang and Mr. C.F. Chang who helped to prepare the manuscript. Thanks finally to J.C. Lee, J.C. Hu and three reviewers (F.K. Brunner, J. Chery, and T. Seno) for their valuable comments and suggestions. This study was financially supported by Academia Sinica and the National Science Council of the Republic of China under grant No. NSC 84-2111-M-001-014. This is a contribution of Earth Sciences, Academia Sinica, IESEP97-004.

References

Angelier, J., Barrier, E. and Chu, H.T., 1986. Plate collision and paleostress trajectories in a fold-thrust belt: the Foothills of Taiwan. Tectonophysics, 125: 161–178.

Angelier, J., Bergerat, F., Chu, H.T. and Lee, T.Q., 1990. Tectonic analysis and the evolution of a curved collision belt: the Hsüehshan Range, northern Taiwan. Tectonophysics, 183: 77–96.

Angelier, J., Lee, J.C., Chu, H.T., Lu, C.Y., Fournier, M., Hu, J.C., Lin, N.T., Deffontaines, B., Delcaillau, B., Lacombe, O. and Lee, T.Q., 1995. Crustal extension in an active orogen: Taiwan (extended abstract). International Conference and 3rd Sino–French Symposium on Active Collision in Taiwan, 22–23 March 1995, Taipei, pp. 25–32.

Barrier, E. and Angelier, J., 1986. Active collision in eastern Taiwan: the Coastal Range. Tectonophysics, 125: 39–72.

Barrier, E., Angelier, J., Chu, H.T. and Teng, L.S., 1982. Tectonic analysis of compressional structure in an active collision zone: the deformation of Pinanshan Conglomerates, eastern Taiwan. Proc. Geol. Soc. China, 25: 123–138.

Biq, C.C., 1972. Dual trench structure in the Taiwan–Luzon region. Proc. Geol. Soc. China, 15: 65–75.

Bowin, C., Lu, R.S., Lee, C.S. and Schouten, H., 1978. Plate convergence and accretion in the Taiwan–Luzon region. Am. Assoc. Pet. Geol. Bull., 62: 1645–1672.

Brunner, F.K. and Welsch, W.M., 1993. Effects of the troposphere on GPS measurements. GPS World, 4: 42–51.

Chen, R.C., Huang, S.T., Shen, H.C. and Chi, W.R., 1994. The structural geology relating to petroleum habitats of the Kuanyin Uplift and its neighboring basins. Pet. Geol. Taiwan, 29: 75–107.

Chou, J.T., 1969. A petrographic study of the Mesozoic and Cenozoic rock formations in the Tungliang well TL-1 of the Penghu Islands, Taiwan, China. U.N. ECAFE Comm. for Coordination of Joint Prospecting for Mineral Resources in Asia Offshore Areas (CCOP), Tech. Bull., 2: 97–115.

Davis, J.L., Prescott, W.H., Svarc, J.L. and Wendt, K., 1989. Assessment of Global Positioning System measurements for studies of crustal deformation. J. Geophys. Res., 94: 13635–13650.

Dixon, T.H., 1991. An introduction to the Global Positioning System and some geological applications. Rev. Geophys., 29: 249–276.

Hager, B.H., King, R.W. and Murray, M.H., 1991. Measurement of crustal deformation using the Global Positioning System. Annu. Rev. Earth Planet. Sci., 19: 351–382.

Ho, C.S., 1976. Foothills tectonics of Taiwan. Bull. Geol. Surv. Taiwan, 25: 9–28.

Ho, C.S., 1982. Tectonic Evolution of Taiwan. Explanatory text of the tectonic map of Taiwan, Ministry of Economic Affairs, R.O.C., 126 pp.

Ho, C.S., 1986. A synthesis of the geologic evolution of Taiwan. Tectonophysics, 125: 1–16.

Hopfield, H.S., 1971. Tropospheric effect on electromagnetically measured range: prediction from surface weather data. Radio Sci., 6: 357–367.

Hsieh, S.H. and Hu, C.C., 1972. Gravimetric and magnetic studies of Taiwan. Pet. Geol. Taiwan, 10: 283–321.

Hsu, T.L., 1976. Neotectonics of the Longitudinal Valley, eastern Taiwan. Bull. Geol. Surv. Taiwan, 25: 53–62.

Hu, J.C., Angelier, J., Yu, S.B. and Lu, C.Y., 1995. An interpretation of the GPS velocity field of southern Taiwan based on numerical modelling (extended abstract). International Conference and 3rd Sino–French Symposium on Active Collision in Taiwan, 22–23 March 1995, Taipei, pp. 141–149.

Huang, C.Y., Shyu, C.T., Lin, S.B., Lee, T.Q. and Sheu, D.D., 1992. Marine geology in the arc–continent collision zone off southeastern Taiwan: implications for late Neogene evolution of the Coastal Range. Mar. Geol., 107: 183–212.

Kimura, M., 1985. Back-arc rifting in the Okinawa Trough. Mar. Pet. Geol., 2: 222–240.

Liu, C.S., Lundberg, N., Reed, D.L. and Huang, Y.L., 1993. Morphological and seismic characteristics of the Kaoping Submarine Canyon. Mar. Geol., 111: 93–108.

Lu, C.Y. and Malavieille, J., 1994. Oblique convergence, indentation and rotation tectonics in the Taiwan Mountain Belt: insights from experimental modelling. Earth Planet. Sci. Lett., 121: 477–494.

Matsumoto, R., 1965. Some molluscan fossils from the buried Cretaceous of western Taiwan. Pet. Geol. Taiwan, 4: 1–24.

Prescott, W.H., 1981. The determination of displacement fields from geodetic data along a strike-slip fault. J. Geophys. Res., 86: 6067–6072.

Rothacher, M., Beutler, G., Gurtner, W., Bockmann, E. and Mervart, L., 1993. Documentation for Bernese GPS software v.3.4. Astronomical Institute, University of Berne, 247 pp.

Savage, J.C. and Prescott, W.H., 1973. Precision of geodolite distance measurements. J. Geophys. Res., 78: 6001–6008.

Seno, T., 1977. The instantaneous rotation vector of the Philippine Sea plate relative to the Eurasian plate. Tectonophysics, 42: 209–226.

Seno, T., Stein, S. and Gripp, A.E., 1993. A model for the motion of the Philippine Sea plate consistent with NUVEL-1 and geological data. J. Geophys. Res., 98: B17941–B17948.

Suppe, J., 1980. Imbricate structure of Western Foothills belt, south-central Taiwan. Pet. Geol. Taiwan, 17: 1–16.

Suppe, J., Hu, C.T. and Chen, Y.J., 1985. Present-day stress direction in western Taiwan inferred from borehole elongation. Pet. Geol. Taiwan, 21: 1–12.

Teng, L.S., 1990. Geotectonic evolution of late Cenozoic arc–continent collision in Taiwan. Tectonophysics, 183: 57–76.

Tsai, Y.B., 1986. Seismotectonics of Taiwan. Tectonophysics, 125: 17–37.

Tsai, Y.B., Teng, T.L., Chiu, J.M. and Liu, H.L., 1977. Tectonic implications of the seismicity in the Taiwan region. Mem. Geol. Soc. China, 2: 13–41.

Wu, F.T., 1978. Recent tectonics in Taiwan. J. Phys. Earth, 26, S265–S299.

Yeh, Y.H., Barrier, E., Lin, C.H. and Angelier, J., 1991. Stress tensor analysis in the Taiwan area from focal mechanisms of earthquakes. Tectonophysics, 200: 267–280.

Yu, S.B. and Chen, H.Y., 1994. Global Positioning System measurements of crustal deformation in the Taiwan arc–continent collision zone. TAO, 5: 477–498.

Yu, S.B. and Lee, C., 1986. Geodetic measurement of horizontal crustal deformation in eastern Taiwan. Tectonophysics, 125: 73–85.

Yu, S.B. and Liu, C.C., 1989. Fault creep on the central segment of the Longitudinal Valley fault, eastern Taiwan. Proc. Geol. Soc. China, 32: 209–231.

Yu, S.B. and Yu, G.K., 1991. Present-day crustal deformation in the Longitudinal Valley area, eastern Taiwan. TAICRUST Workshop Proc., Taipei, pp. 185–195.

Yu, S.B., Jackson, D.D., Yu, G.K. and Liu, C.C., 1990. Dislocation model for crustal deformation in the Longitudinal Valley area, eastern Taiwan. Tectonophysics, 183: 97–109.

Yu, S.B., Yu, G.K., Kuo, L.C. and Lee, C., 1992. Crustal deformation in the southern Longitudinal Valley area, eastern Taiwan. J. Geol. Soc. China, 35: 219–230.

Yu, S.B., Chen, H.Y. and Kuo, L.C., 1995. Velocity field of GPS stations in the Taiwan area (extended abstract). International Conference and 3rd Sino–French Symposium on Active Collision in Taiwan, 22–23 March, 1995, Taipei, pp. 317–327.